Plasma Phys. Control. Fusion **41** (1999) B351–B365. Printed in the UK PII: S0741-3335(99)07625-3

Transport and MHD studies at high T_e in FTU tokamak

S Cirant†, A Airoldi†, L Bertalot‡, G Bracco‡, A Bruschi†, P Buratti‡, G Cenacchi§, R Coelho‖, F Crisanti‡, B Esposito‡, L Gabellieri‡, F Gandini†, G Granucci†, E Lazzaro†, H Krögler‡, S Nowak†, D Pacella‡, L Panaccione‡, G Ramponi†, A Simonetto†, C Sozzi†, O Tudisco‡, M Zerbini‡, F Alladio‡, B Angelini‡, M L Apicella‡, G Apruzzese‡, E Barbato‡, A Bertocchi‡, M Borra‡, G Buceti‡, A Cardinali‡, C Centioli‡, R Cesario‡, P Chuilon‡, S Ciattaglia‡, V Cocilovo‡, R De Angelis‡, D Frigione‡, G Gatti‡, E Giovannozzi‡, M Grolli‡, F Iannone‡, M Leigheb‡, G Maddaluno‡, M Marinucci‡, G Mazzitelli‡, P Micozzi‡, P Orsitto‡, M Panella‡, V Pericoli‡, L Pieroni‡, S Podda‡, G B Righetti‡, F Romanelli‡, S E Segre¶, S Sternini‡, N Tartoni‡, A A Tuccillo‡, V Vitale‡, G Vlad‡, V Zanza‡ and F Zonca‡

† Istituto di Fisica del Plasma del CNR, Associazione EURATOM-ENEA-CNR, Via R.Cozzi 53, Milano, Italy

‡ Centro Ricerche Energia ENEA-Frascati - Associazione EURATOM-ENEA-CNR sulla Fusione, Frascati, Italy

§ Centro Ricerche Energia ENEA, Via Don Fiammelli 2, Bologna, Italy

‖ Centro Fusão Nuclear, 1049-001, Lisboã, Portugal, Assoc. Euratom-IST

¶ Università di Roma 'Tor Vergata', Roma, Italy

Received 18 June 1999

Abstract. Magnetohydrodynamic (MHD) activity and energy transport at rational-q surfaces is analysed on the basis of experimental results on current density profile control obtained with localized electron cyclotron resonance heating (ECRH) on FTU tokamak. The MHD response, in particular 2/1 and 1/1 modes, to ECRH is in agreement with expectations from a theoretical model including resistive wall braking and toroidal mode coupling. It is also shown that the magnetic shear at $r_{q=1}$ could control $m = 1$ mode saturation and magnetic reconnection. Heating results with ECRH at steady state indicate that transport enhancement is the dominant effect on confinement at the $q = 2$ surface, and suggest that conduction and convection inside the asymmetric $m = 1$ island should both be taken into account for a proper description of the thermal response to localized ECRH.

1. Introduction

The magnetic structure inside the plasma column is generally understood to have a direct impact on energy confinement, both positive with the formation of transport barriers when low or inverted magnetic shear conditions are established [1], and negative with the formation of a thermal bridge across the full width of magnetohydrodynamic (MHD) islands [2]. An empirical model which locates narrow thermal barriers close to a selected choice of low-order rational-q magnetic surfaces has been proposed to explain the results of experiments on RTP tokamak with electron cyclotron resonance heating (ECRH) overwhelming the ohmic power input [3].

0741-3335/99/SB0351+15$30.00

A special role is played by the $m = 1$, $n = 1$ mode, and the related sawtooth-like disruptions, because core parameters are in this case directly affected. Recently, it has been shown [4, 5] that heat convection inside the $m = 1$ cell should be considered together with diffusion in the energy transport and profile shaping at the plasma centre.

Strong and localized ECRH is used to predominantly excite only a few of the many links in the action/reaction chain governing transient and steady-state profiles. Controlled resistivity re-shaping may induce a response in a known direction of the q-profile and MHD activity. Observable correlated changes in the locally stored energy density and confinement properties are used to gauge discontinuities (barriers or bridges?) in energy transport near rational-q surfaces, and to challenge the standard modelling of the MHD contribution to energy transport.

The paper discusses first the MHD activity as observed in high-temperature, ECRH plasmas, and then analyses its relation with energy confinement, taking further advantage of the absorption properties of EC waves.

2. ECRH during current ramp-up and at current flat-top

Plasmas with very high electron temperatures have been sustained in the high-field FTU tokamak by localized absorption of EC waves at 140 GHz, the fundamental resonance, in the O-mode.

Temperature values above 10 keV are obtained with central heating at $P_{\mathrm{ECRH}} = 800$ kW, $n_{\mathrm{e,line}} \approx 0.35 \times 10^{20}$ m^{-3} during current ramp-up (figure 1) from 0 to 700 kA at a rate of 5 MA s^{-1} [6], in the sawtooth-free phase characterized by $q_{\min} > 1$. Due to the very large absorbed power density (in excess of 100 MW m^{-3} according to ray-tracing calculations [7]) and the relatively low electron density, kinetic effects on the bulk of the electron energy distribution function are foreseen [8]. In fact, the emitted EC spectrum is in good agreement with these expectations [6], confirming the need for a careful interpretation of the ECE measurements in terms of 'temperature' in these conditions. Figure 1 shows the peak temperature given by the second harmonic ECE, measured by a Michelson interferometer,

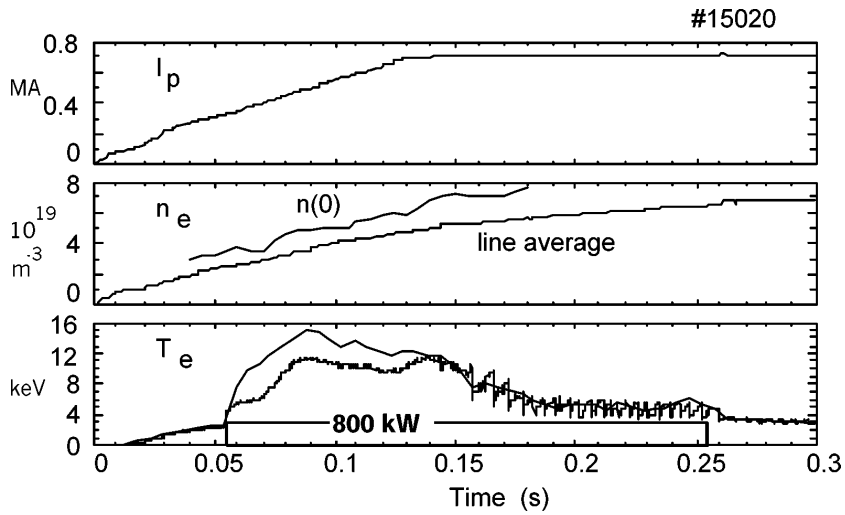

Figure 1. Plasma current, electron density (line average and peak), and electron temperature with central ECRH at 800 kW during current ramp-up.

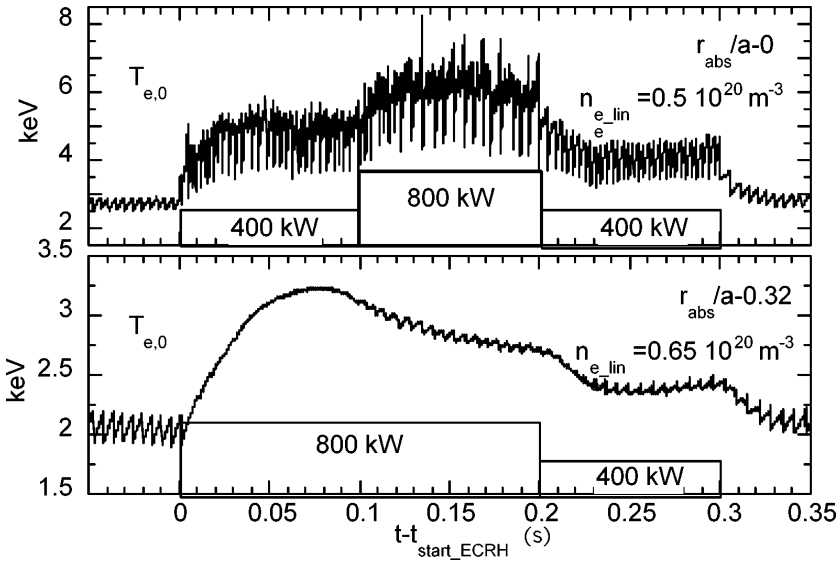

Figure 2. Peak electron temperature for on-axis (top) and off-axis (bottom) ECRH at current flat-top. Sawteeth are larger and faster when heating at the centre, and may be stabilized when EC power is absorbed at about the inversion radius.

together with the temperature measured by one channel of an ECE polychromator tuned at less than 2 cm away. Both temperatures are calculated from the measured ECE assuming a Maxwellian plasma. Although the peak value should be corrected for kinetic effects from ≈14 keV to ≈12 keV, the profile still remains extremely peaked until the onset of sawteeth.

The target plasma for ECRH experiments at the current flattop is always sawtoothing, even at the relatively low current of 350–400 kA, in spite of the large value of the edge safety factor $q_a \approx 6$. Operation at low current is necessary to keep the ECRH power ($P_{\mathrm{ECRH}} = 800$ kW, coupled to the plasma) well in excess of the ohmic input, which is $P_{\mathrm{oh}} \approx 400$ kW in the purely ohmic phase and $P_{\mathrm{oh}} \approx 200$ kW during ECRH.

On-axis ECRH strongly increases the sawtooth amplitude, from $\Delta T_{\mathrm{e,0\_ECRH}} \approx 0.3$ keV to $\Delta T_{\mathrm{e,0\_ECRH}} \approx 2$ keV, and shortens the period ($\tau_{\mathrm{st\_ECRH}} \approx 0.6\ \tau_{\mathrm{st\_oh}}$) [9–11]. In spite of the periodic full reconnections, limiting the maximum achievable central heating, remarkable electron temperatures have still been observed. As shown in figure 2, at $n_{\mathrm{e,line}} = 0.6\times10^{20}$ m^{-3}, $P_{\mathrm{tot}} \approx 1000$ kW, $T_{\mathrm{e,0}}$ increases up to ≈7.5 keV before the sawtooth crash. The average central temperature, taken over several sawtooth periods, reaches $\langle T_{\mathrm{e,0}} \rangle \approx 6.5$ keV.

With the EC absorption layer shifted off-axis, either by changing the toroidal field or by tilting the beam axis, a variety of cases is observed as described in the following. As shown in figure 2, the peak temperature decreases with increasing distance of the absorption layer from the magnetic axis r_{abs}, and in some conditions sawteeth are stabilized.

Since the cut-off density for the ordinary mode, at the fundamental resonance of 140 GHz, is $n_{\mathrm{e,cut\text{-}off}} = 2.4 \times 10^{20}$ m^{-3}, ECRH can be performed in a density range where significant e–i energy exchange is expected [9, 12]. This feature can be used to help the flattening of the electron temperature and current density profile with off-axis ECRH. At $n_{\mathrm{e,0}} \approx 1 \times 10^{20}$ m^{-3}, the residual ohmic power density at the centre may be insufficient to sustain radiation losses and the e–i energy transfer, and a hollow electron temperature profile develops (figure 3) [13]. The various power fluxes have been estimated by modelling the discharges with a diffusive transport code.

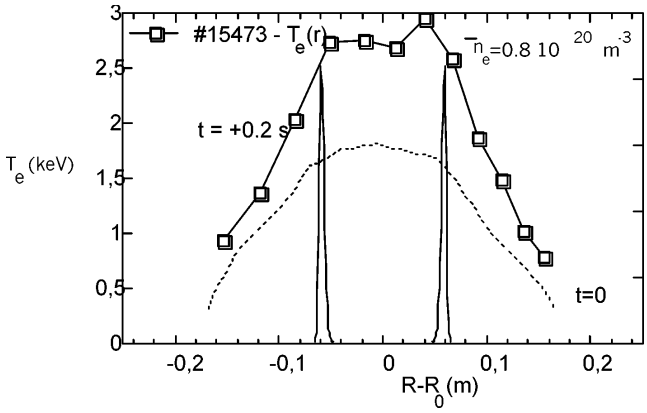

Figure 3. At high electron density, off-axis ECRH ($P_{\rm abs}$ from beam-tracing is shown, a.u.) and e–i thermal exchange produce hollow temperature profiles.

In order to correctly interpret the effects of profile reshaping with ECRH, it is most important to have a good estimate of the position $r_{\rm abs}$ of the directly heated volume with respect to the plasma axis. Beam-tracing calculations, based on the measured electron density and temperature, and on equilibrium reconstruction, provide an estimate of the EC wave absorption along the major radius $R_{\rm abs}$, which was verified with measurements. The fast ECE polychromator is used for the comparison, looking for the channels with the largest jump in the heating rate $\mathrm{d}(n_{\rm e}T_{\rm e})/\mathrm{d}t$ at switching $P_{\rm ECRH}$ on. As shown in figure 4, ray-tracing and ECE measurements agree in the estimate of $R_{\rm abs}$ within 1 cm, also taking into account that the polychromator channels are separated by $\approx$2 cm.

Within the range of the explored plasma parameters, the global energy confinement time scales during ECRH are in good agreement with ITER89P, L-mode (figure 5) [13].

3. MHD response to localized ECRH

Since there is no direct measure of the local current density and the magnetic structure inside the plasma column, the MHD activity is observed in FTU tokamak through its effects on the electron temperature.

Central ECRH shortens the reconnection period with respect to the ohmic plasma, in spite of the higher electron temperature and longer resistive diffusion times. By shifting the EC absorption from the centre to $r_{\rm abs} \approx r_{\rm inv}$ [11, 14], where $r_{\rm inv}$ is the sawtooth inversion radius, the repetition rate can be slowed down to much less than the ohmic value. When $r_{\rm abs} \approx r_{\rm inv}$, the response is extremely sensitive to the actual value of $r_{\rm abs}$: complete $m = 1$ stabilization can be obtained with an outward shift of $r_{\rm abs} \approx 1$ cm (less than 5% of the minor radius), or fast reconnections may disappear but with a persistent and stable $m = 1$ oscillation, with a further outward shift of $\approx$1 cm. All possible cases, from sawtoothing to fully stabilized plasmas, are shown in figure 6.

Stabilization is prompt, occurring in times much shorter than the resistive diffusion time across the $q = 1$ rational surface. Furthermore, stabilization is transient in many cases, both because the electrodynamic reaction to the fast change in the resistivity profile drives an internal time-dependent inductive current distribution which can contribute to stabilization [11], and because the shift following the plasma pressure increase might move the absorption layer away from the point effective for stabilization [10]. At the switching off of the ECRH power,

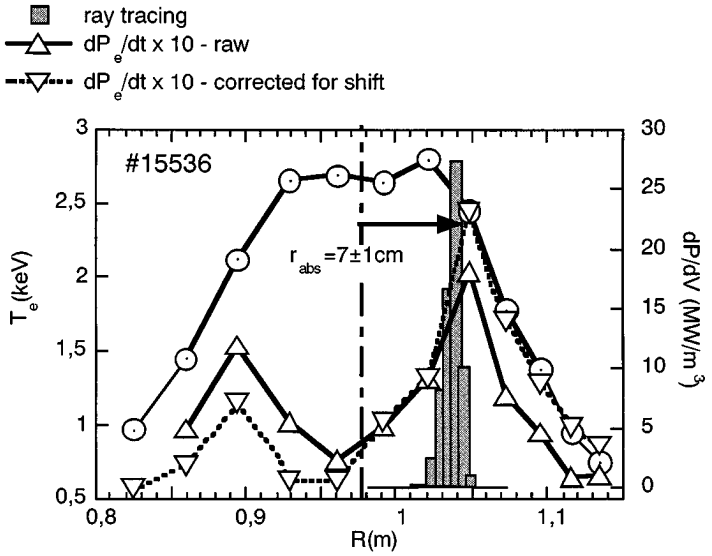

Figure 4. The estimate of the absorbing layer from beam-tracing agrees with the position where the heating rate at ECRH-ON is faster.

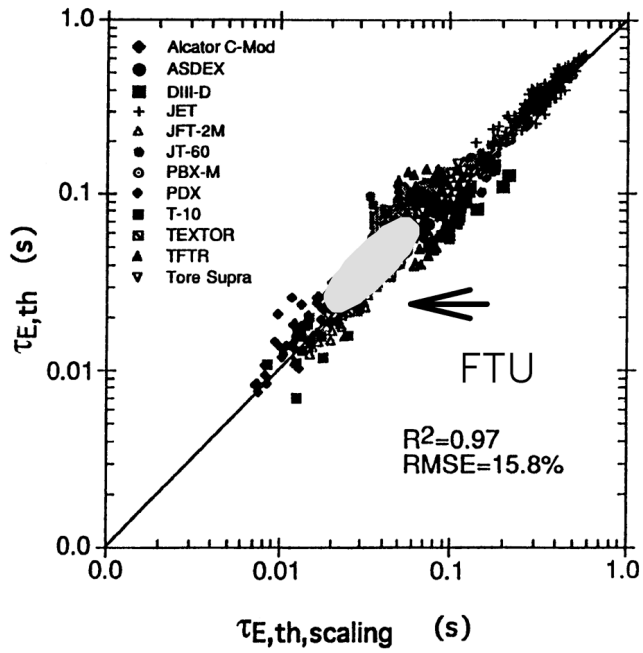

Figure 5. The global energy content with ECRH at steady-state scales in fair agreement with ITER L-mode scaling laws. FTU data with ECRH are compared in the figure with ITER97 scaling [22].

a saturated $m = 1$ oscillation first reappears, which eventually grows until reconnections start again (figure 7).

The great sensitivity of the stabilization to r_{abs} and the fast time scale on which it occurs, both suggest that the effect is due to a change in the local parameters, such as the magnetic

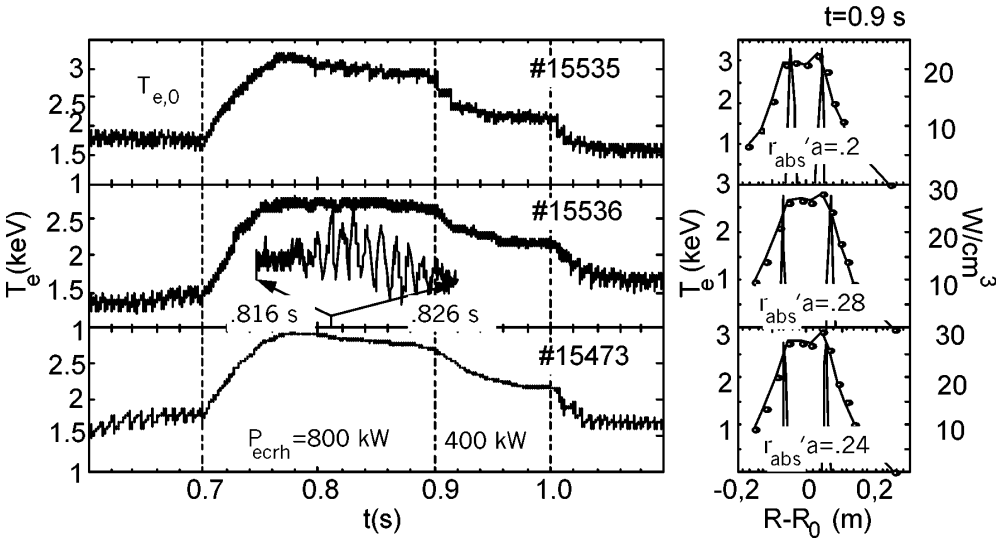

Figure 6. Central electron temperature (left) and temperature profiles at steady-state (right), for three discharges with ECRH aiming at $m = 1$, $n = 1$ mode stabilization. Within a shift ≈2 cm (8% of the minor radius), all possible effects are observed, from sawtoothing to a fully stabilized plasma.

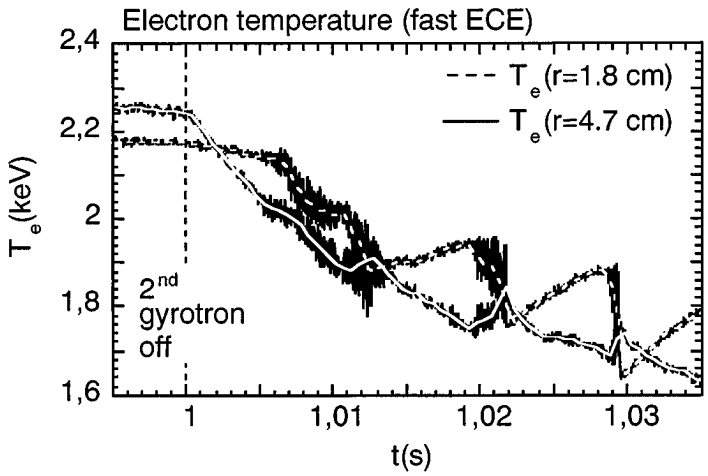

Figure 7. Electron temperature (fast ECE measurements) at two radial points close to the plasma centre. As the 1/1 mode reappears after stabilization, core confinement is degraded.

shear at $r_{q=1}$, rather than to a change in the whole current profile in the central region and in q_0 [11, 14, 15]. This point will be discussed in detail in a later section.

During operation at low current ($I_p \approx 350$ KA), the ohmic plasma may sustain a persistent $m = 2$, $n = 1$ temperature oscillation, located at $r \approx r_{q=2}$. By applying ECRH at $r_{abs} \approx r_{q=1}$ for $m = 1$ stabilization, the $m = 2$ mode is further destabilized (figure 8), probably by the local increase of the poloidal β. Depending on its frequency, the enhanced thermal oscillation persists during the whole ECRH pulse (figure 8, bottom), or may slow down and disappear because the mode stops rotation (figure 8, top, and figure 9). As discussed in a later section, the observed frequency evolution as the magnetic island grows, and eventually the mode locking,

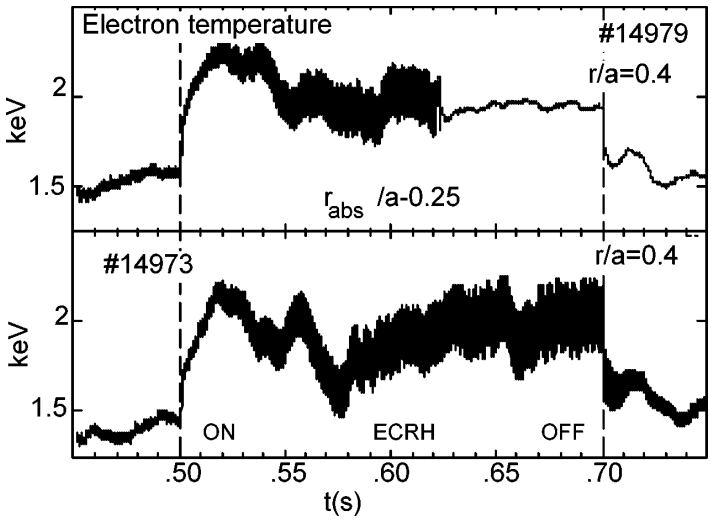

Figure 8. ECRH at $r_{\rm abs} \approx r_{\rm inv}$ may further destabilize pre-existing tearing modes $m = 2$, $n = 1$. The figure shows the electron temperature (ECE diagnostic) at $r \approx r_{q=2}$. The mode may eventually become locked (top) by the wall braking torque (cf figure 9), or may continue to exist for the whole pulse length depending on its frequency.

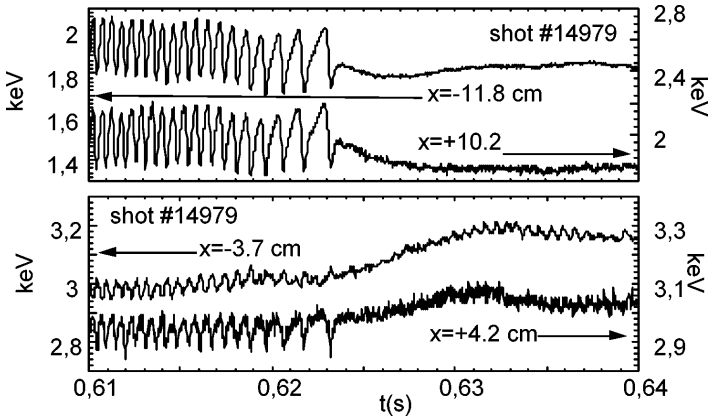

Figure 9. Toroidal geometry may couple the 2/1 and 1/1 modes, as shown by temperature fluctuations at $r \approx r_{q=2}$ (top) and at $r \approx r_{q=1}$ (bottom). When 2/1 locks to the walls, 1/1 continues free but at a lower amplitude.

are well explained by inertial effects and by considering the braking torque applied to the rotating magnetic island by image currents in the resistive walls.

Destabilization of the 2/1 mode may drive an increase in the 1/1 mode amplitude, as predicted by the toroidal coupling of modes with nearby m-order [15]. The two modes are experimentally observed to evolve at the same frequency, until 2/1 locks and 1/1 continues with reduced amplitude, free to oscillate at its natural frequency (figure 9).

4. Theoretical modelling of MHD during ECRH

The evolution of the $m = 1$ mode during ECRH can be described by a model for the growth rate in the linear and nonlinear regimes. The relevant instability regime for the parameter range of the experiments of sawtooth stabilization ($n_e \approx 1 \times 10^{20}$ cm^{-3}, $T_e \approx 2$–5 keV, $T_i \approx 1$ keV, $0.1 < s_1 < 0.5$) is the ion kinetic regime [16]. In this case, neglecting diamagnetic frequency effects, the characteristic linear growth rate γ_L of the internal $m = 1$ kink mode is:

$$\gamma_L = \left(\frac{2(1+\tau)}{\pi}\right)^{2/7} \left(\frac{\rho_i}{r_1}\right)^{4/7} S^{-1/7} s_1^{6/7} \tau_A^{-1} \tag{1}$$

where $\tau = T_e/T_i$, τ_A is the Alfvén time, ρ_i the ion Larmor radius, S is the Lundquist number, and s_1 is the magnetic shear at $r_1 = r_{q=1}$. The inclusion of diamagnetic effects in the dispersion relation leads to a threshold for stability expressed in terms of the electron and ion diamagnetic frequencies by:

$$\gamma_L > c^{*-1}(\omega_{\mathrm{dia,e}}\omega_{\mathrm{dia,i}})^{1/2} \tag{2}$$

where $\omega_{\mathrm{dia\ e,i}} = T_{\mathrm{e,i}} L_{\mathrm{p_{e,i}}}^{-1}/eBr_1$, and c^* is a numerical factor which depends on local plasma parameters and profiles.

Values of the parameter $c^* \sim 1$ are adjusted to fit the experimental sawtooth period in the ohmic phase. When the growth of the $m = 1$ Lagrangian fluid displacement is unhindered by saturation effects, the instability proceeds to full reconnection and the practical condition for triggering the sawtooth crash that follows from equations (1) and (2) may be written in terms of a critical shear at the $q(r_1) = 1$ surface $s_{cr}(T_{e,i}, L_{n_{e,i}}, L_{p_{e,i}}, \beta_e)$:

$$s_1 \geqslant c^{*-7/6} \tau_A^{7/6} (\omega_{\mathrm{dia,e}}\omega_{\mathrm{dia,i}})^{7/12} (\pi T_i/2(T_i + T_e))^{1/3} (r_1/\rho_i)^{2/3} (\tau_{res}/\tau_A)^{1/6} \tag{3}$$

where all quantities are to be evaluated at the $q = 1$ surface and τ_{res} is the resistive time. Numerical simulations implementing this criterion reproduce satisfactorily the sawtooth period during ECRH [14].

An interesting case is that in which the conditions for the sawtooth reconnection exist, but transient stabilization is immediately obtained as the ECRH is turned on and leads to a finite-amplitude nonlinear $m = 1$ mode (figure 6). For a possible explanation of the observed MHD behaviour, we construct a model of transition from the linear instability regime to a nonlinear one dominated by the modifications of pressure gradient, resistivity and magnetic shear caused by the localized ECH power.

The evolution of the amplitude $\xi_0(t) = W(t)/2$ can be described symbolically by [16]:

$$\dot{\xi}_0 = \gamma_L \xi_0 + \gamma_{NL}(\xi_0)\xi_0 + \gamma_I \xi_0. \tag{4}$$

The linear growth rate is valid for Lagrangian displacements $|\xi_0| \leqslant \rho_i(1 + T_e/T_i)^{1/2}$ when the conditions of critical shear are met. The ideal kink growth rate $\gamma_1 \approx -q'(r_s)\lambda_H \tau_A^{-1}/\sqrt{3}$ is relevant for $\lambda_H = -(3\pi r_s^2/q'R^2)\ (\beta^2_{\mathrm{Bussac}} - \beta_p^2) < 0$ [17].

We define here a nonlinear growth rate as $\gamma_{NL}(\xi_0) = \dot{\xi}_0/\xi_0 = \dot{W}/W$. For large displacements [16], γ_{NL} is meant to take over γ_L and is calculated from a model based on Maxwell's equations and a sufficiently general Ohm's law, in the reduced MHD (RMHD) description of fields in terms of flux and stream functions for the single helicity $m = 1$ perturbation. It is assumed that $q(0) < 1$ and a Rutherford type equation [18] is deduced for a finite-amplitude (Lagrangian) displacement of an $m = 1$ mode.

We assume a crescent-like structure of the $m = 1$ helical flux contour $\Psi = -(B_0 s_1/2R)[(x^2 - xW\cos\vartheta)H(-x) + x^2 H(x)]$ related to the rigid displacement [18–20] $\xi = (W/2)H(-x)\cos\vartheta$, where $x = r_1 - r$, and the expansion of the resistivity in the neighbourhood of the $q = 1$ surface.

Combining the equations for the pressure, the generalized Ohm's law and the quasineutrality condition $\nabla \cdot \boldsymbol{J} = 0$, with Ampere's and Faraday's laws, suitably integrated over the island, one obtains the balance of all the electromotive forces competing in the reconnection process. The result is an equation for the island width

$$\left(\frac{g_{\rm rec}\tau_{\rm R}}{r_1}\right)\frac{{\rm d}W}{{\rm d}t} = \left\{\left[1 - \frac{(\alpha + \alpha_{\rm H}(t))^2}{s_1^2} g_{\rm PS} - g_{\rm h} F_2(t)\right]\frac{r_1}{(W + g_{\rm d} d_{\rm e}^2/r_1)} - g_\eta\left(\frac{c}{4\pi}\frac{\eta_0'}{\eta_0} + F_1(t)\right)\frac{W}{(W + g_{\rm d} d_{\rm e}^2/r_1)}\right\} \tag{6}$$

where $F_1(t)$, $F_2(t)$ and $\alpha_{\rm H}(t)$ are control terms dependent on the localized RF power pulse. The parameters s_1, $q'r_1$ and $\alpha = 8\pi p' R/B^2$ are the local shear and normalized pressure gradient; the coefficients $g_{\rm rec} \approx 0.3$, $g_{\rm ps} \approx 1$, $g_{\rm h} \approx 10$, $g_\eta = 6.3$ are obtained by nonlinear averaging over the crescent-like $m = 1$ island.

From the (ion) momentum balance equation one obtains a heuristic equation for the rotation frequency of the plasma trapped within the island

$$\frac{\partial \omega}{\partial t} = -\omega\frac{\ln W}{{\rm d}t} - \mu_\perp^{\rm an}\frac{r_1}{W}(\omega - \omega_0). \tag{7}$$

The model predicts qualitatively an $m = 1$ response to ECRH in the nonlinear saturated phase as shown in figure 10. It is shown that an increase in the local normalized β and a drop in the local magnetic shear, of a magnitude compatible with the experimental cases, can compress and stabilize a growing $m = 1$ mode. At fixed r_1, the change of rotation frequency due to inertial effects is limited by viscosity. The theoretical model is in qualitative agreement with the experimental behaviour observed in shot #15536, in which full stabilization is transiently achieved (figure 11(*a*)), followed by a long-lasting $m = 1$ saturated oscillation (figure 11(*b*)).The island pulsation is higher when its width and r_1 are small, and decreases later when the $m = 1$ mode is fully developed.

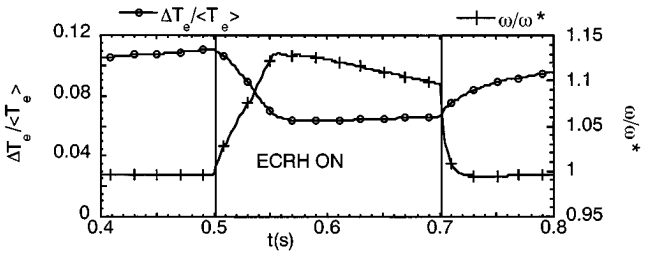

Figure 10. Qualitative reconstruction of the dynamics of a coherent and slowly growing $m = 1$ mode with ECRH. The fractional amplitude and the frequency (normalized to the electron drift frequency) of the MHD oscillations are calculated from equations (6) and (7), using measured plasma parameters and an estimate for the local shear and normalized β evolution given by modelling an EC heated plasma with a time-dependent diffusive transport code. It is shown that an increase in the local normalized β and a drop in the local magnetic shear, compatible with experimental observations, can stabilize a growing instability. At fixed $r_{q=1}$, the change of rotation frequency with the island width due to inertial effects is reduced by viscosity.

In some other cases, as a consequence of a moderate re-shaping of the current density profile induced by the ECRH deposition on the $q = 1$ surface, and of an increase of the local and average $\beta_{\rm p}$, the conditions of marginal stability of background MHD resistive modes with $m = 2$ are altered. We discuss here an interesting case characterized by toroidal coupling and uncoupling events of $m = 1$, $n = 1$ and $m = 2$, $n = 1$ modes associated with wall

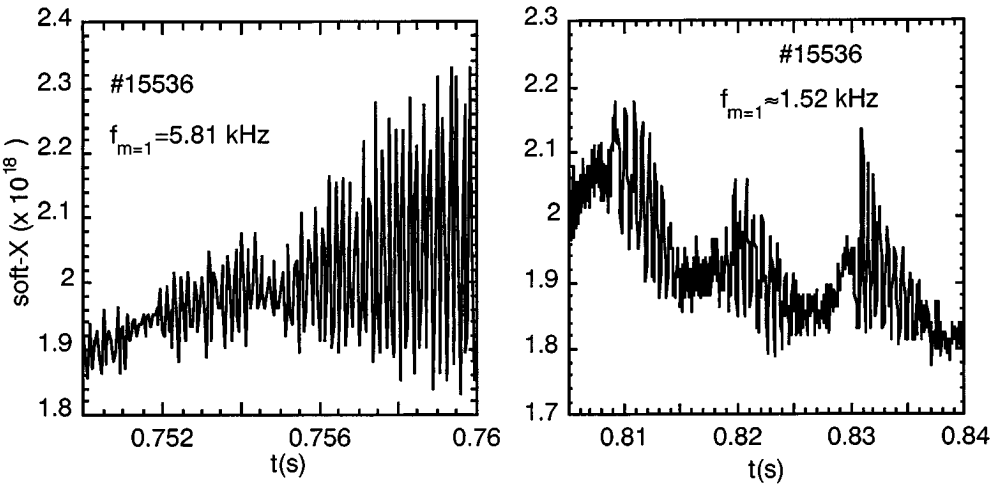

Figure 11. In shot #15536 $m = 1$ instability, after transient stabilization, persists for the whole ECRH pulse (cf figure 6). The frequency is higher when the mode reappears after stabilization (*a*) and $r_{q=1}$ is small, than at later times (*b*) when the mode is close to reconnection.

braking effects. We apply here a theoretical model of the Rutherford type, obtained in the large R/a, RMHD ordering from the quasineutrality condition, Faraday's and Ampere's laws averaged over the island, and the momentum balance equation generalized to account for rotation, interaction with the resistive wall of radius $r = d$ and toroidal coupling with modes of poloidal numbers m, $m \pm 1$. We obtain equations for the island width and frequency:

$$\frac{\mathrm{d}W_m}{\mathrm{d}t} = \frac{r_m^2}{\tau_{R_m}}\left[\Delta'_m + C_{m,m\pm1}\frac{W_{m\pm1}^2}{W_m^2}\cos(\Delta\phi) - f_R(\omega_m\tau_{wm})\right]$$

$$\frac{\mathrm{d}\omega_m}{\mathrm{d}t} = \frac{1}{I_\phi^{(m)}}\left[D_{m,m\pm1}W_{m\pm1}^2W_m^2\sin(\Delta\phi) - W_m^4h_m^2f_1(\omega_m\tau_{wm}) - \omega_m\frac{\mathrm{d}I_\phi^{(m)}}{\mathrm{d}t}\right] - \mu_{\perp m}\frac{r_m}{W_m}(\omega-\omega_m).$$

The nonlinear function $\Delta'_m(W) = \Delta'_{0,m} + \Delta'_{\mathrm{bs},m} - \Delta'_{\mathrm{GGJ},m} - \Delta'_{\mathrm{GGJ},m}$ is an effective stability index appropriately defined for each mode m and includes finite β_p terms [15]. $D_{m,m\pm1}$ and $C_{m,m\pm1}$ are coupling coefficients consistent with momentum balance and $h_m = Br_{sm}q'/16Rq^2$. The functions $f_\mathrm{R}(\nu_m)$ and $f_1(\nu_m)$ represent the real and imaginary part of the response of the wall (of radius d) to the time-dependent magnetic perturbations

$$f(\nu_m) = \frac{2m}{r_{sm}}\left(\frac{r_{sm}}{d}\right)^2\frac{(\nu_m)^2 + \mathrm{i}\nu_m}{1+(\nu_m)^2}$$

for a circular large R/a geometry.

As shown in [15], the model reproduces the frequency behaviour, the coupling of 2/1 and 1/1 modes and the wall locking as observed in experiments (figures 8 and 9).

5. Electron energy transport around rational-q surfaces

The destabilization of the 2/1 tearing mode with ECRH causes a net loss in the global energy content, and the development of large shoulders in the electron temperature steady-state profile

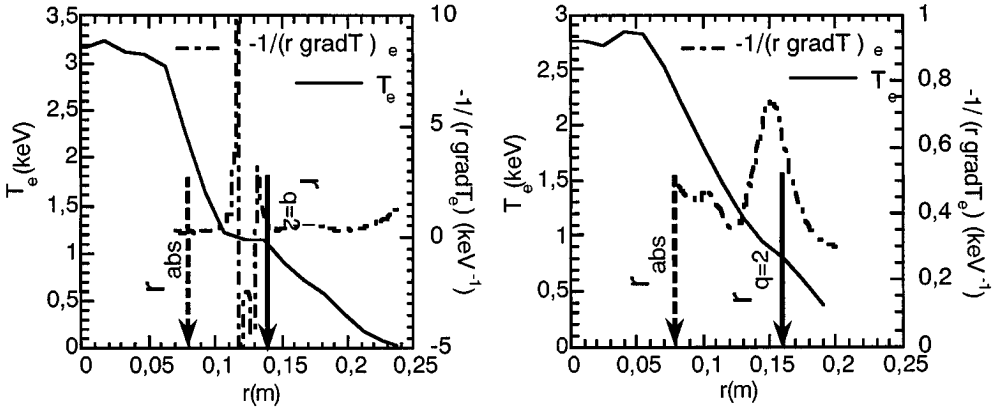

Figure 12. Shoulders are developed on the temperature profile by 2/1 MHD islands, which depend on the island width. The enhanced thermal diffusivity at $r \approx r_{q=2}$ is visible also in discharges apparently free of macroscopic $m = 2$ oscillations (right). In the large island (left) the temperature may not be flat, but slightly increasing towards the outward edge.

at $r \approx r_{q=2}$. In figure 12, the radial plot of $1/(r\nabla T_e)$, roughly corresponding to the local effective thermal diffusivity for $r > r_{abs}$, is shown together with $T_e(r)$. Two discharges are shown, one with and the other without large 2/1 fluctuations. The emerging feature in both cases is a local effective thermal conductivity at $r \approx r_{q=2}$ much higher than elsewhere in the plasma. The local drop in thermal resistance is much stronger in the case of a large island (at the left of the figure, where the measured ∇T_e falls to zero), but remains dominant also in the discharges (at the right of the figure) without large $m = 2$ thermal fluctuations.

The same conclusion is reached by the analysis of the $T_{e,0}$ time evolution with central ECRH during current ramp-up, when rational-q surfaces of progressively lower order enter the discharge in sequence. As shown in figure 13, a large internal disruption due to a 2/1 double tearing mode instability marks the appearance of the $q = 2$ surface inside the plasma. The peak temperature does not fully recover after disruption, indicating that net confinement degradation is associated with rational-q surfaces. Core confinement improves as q_{min} approaches unity, at $t \approx 0.14$ s in figure 13. The sudden rise of the central temperature and pressure at constant ECRH power occurs when the fluctuation-free region corresponding to the gap between $q = 1$ and the nearest unstable rational-q value enters the plasma core gap, which is particularly large in flat or shear-reversed configurations [21]. The central pressure falls again as sawteeth set in ($t \approx 0.16$ s in the figure).

It is worth noticing that the T_e profile is not strictly flat inside the large 2/1 island but, as observed elsewhere [2], it shows a non-intuitive positive slope towards the outward edge. This fact points to the complexity of thermal transport when the symmetry of nested flux surfaces is broken, with the possible onset of convective transport and fluid motion inside the magnetic island [4].

Central heating dependence with r_{abs} can be a monitor of the presence of discontinuities in the effective thermal diffusivity at $r \approx r_{q=1}$ [3]. In the case of a narrow barrier with a thermal resistance much higher than the surrounding plasma, the peak temperature at the steady state would be insensitive to the actual position of the absorbing layer, provided that it is located inside the volume confined by the barrier itself. Figure 14 shows the electron pressure increase $\Delta P_{e,0}$ at the centre for discharges with different position of the EC absorbing layer and different P_{ECRH}. The actual value of $\Delta P_{e,0}$ is averaged over several sawtooth cycles,

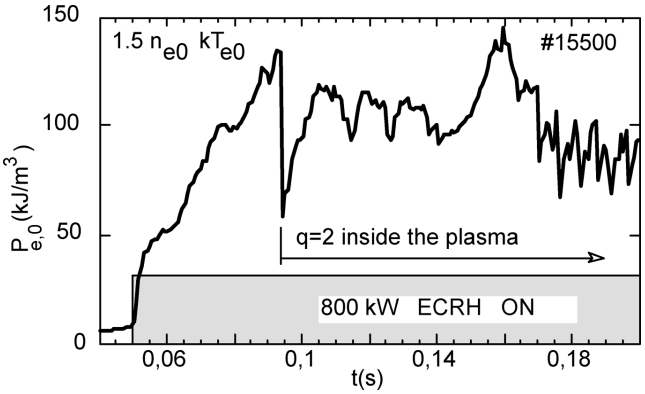

Figure 13. Peak pressure evolution during current ramp-up with central ECRH. The appearance of a rational-q surface is marked by a strong internal disruption due to the double tearing mode. After 2/1 disruption ($\approx$0.1 s), the central energy density does not fully recover.

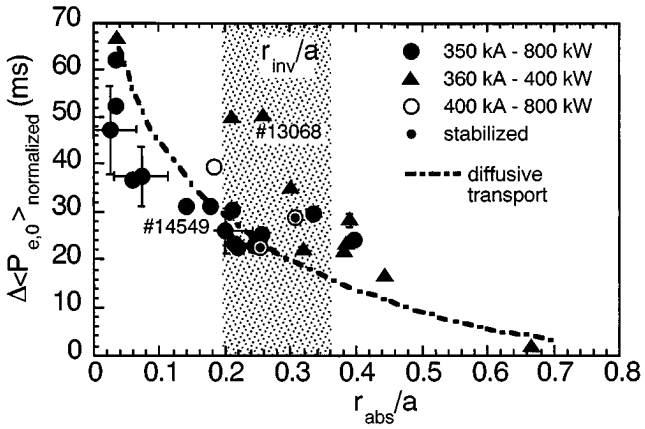

Figure 14. Central heating versus the position of the absorption layer. The pressure increase is normalized to P_{ECRH} and to the plasma volume. Dots mark the discharges with full $m = 1$ stabilization with off-axis ECRH (at 400 kW, 400 kA). The dashed line shows the trend expected with smooth diffusivity (from power balance at 800 kW).

and it is normalized to the coupled ECRH power and the total plasma volume. The error bars account for ± 1 cm uncertainty in r_{abs}, and for the sawtooth amplitude and central density error in the estimate of the average pressure increase. It should be noted, however, that each independent value of r_{abs} and r_{inv} is affected by the error, but, looking directly at the response of fast ECE polychromator channels, the relative position between r_{abs} and r_{inv} is quite certain. In shot #13068, for example, the channel where the heating rate is faster at $t = t_{\mathrm{ECRH\_ON}}$ is also close to the separatrix between positive and inverted sawteeth, and therefore $r_{\mathrm{abs}} \approx r_{\mathrm{inv}}$. The dashed line shows, for comparison, the $\Delta P_{\mathrm{e},0}$ calculated assuming diffusive transport, with a diffusivity consistent with the power balance analysis at $P_{\mathrm{ECRH}} = 800$ kW. The shadowed area covers the interval of r_{inv}/a observed in the different discharges included in the plot.

From the data shown in figure 14, a clear-cut conclusion concerning the presence of discontinuities in radial transport is masked by the large scattering of the observed $\Delta P_{\mathrm{e},0}$, particularly when $r_{\mathrm{abs}} \approx r_{\mathrm{inv}}$, which is larger than the error bars. Let us consider two shots, one characterized by an increase in the central pressure above what is expected by smooth

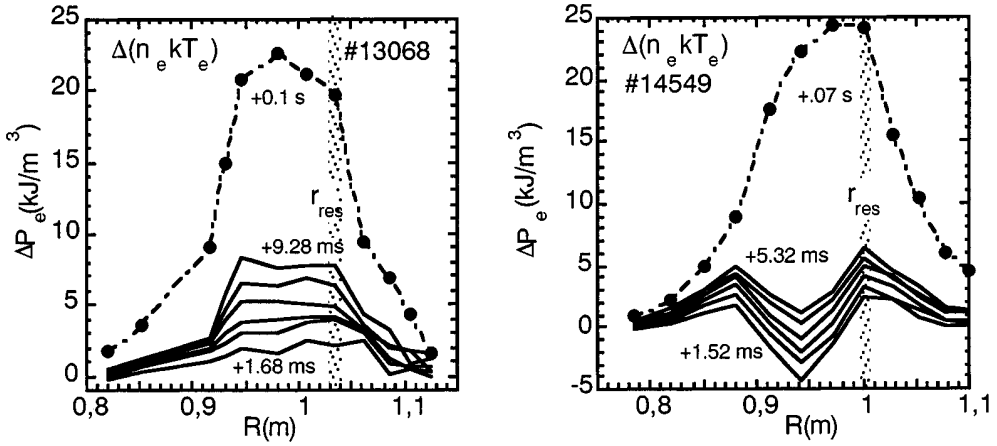

Figure 15. Pressure profile evolution after ECRH switching-ON. As expected from diffusive transport, the profile for #14549 is hollow at the beginning and fills up at longer times. For #13068, the energy density profile is rapidly flattened, as if inward heat convection were active. Also, at steady-state the energy content is the same for the two discharges, but P_{ECRH} in #14549 is twice than in #13068.

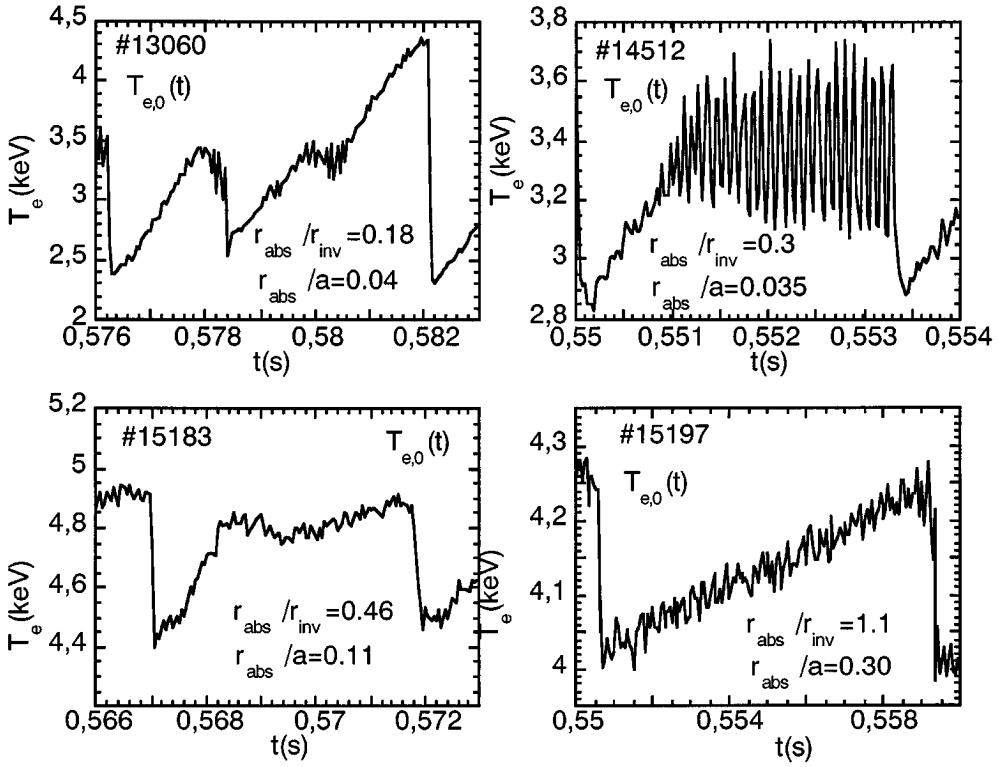

Figure 16. Central temperature with ECRH at different positions with respect to the 1/1 MHD island. The sawtooth shape varies very much with position, until a regular sawtooth reappears as the absorption is shifted well outside the inversion radius.

diffusive transport (#13068), and the second one closer to the diffusive trend (#14549). In both cases $r_{\mathrm{abs}} \approx r_{\mathrm{inv}}$.

In figure 15 the evolution of the temperature profiles is shown at instants close to $t_{\mathrm{ECRH\_ON}}$ for these two discharges. The profile is hollow for #14549, as expected assuming a diffusive transport; instead it is flat from the very beginning for #13068. This suggests the presence of a heat convection mechanism of the absorbed ECRH power, which is active only in specific conditions when the absorption is localized in the region of interest by the 1/1 island, and causes the scattering observed in $\Delta P_{\mathrm{e},0}$. A possible cause is the convective transport inside the $m = 1$ cell, associated with localized ECRH [4].

A further element in this direction is given by the fast time response of the central temperature during ECRH, which depends on the position of the absorbing layer inside the $m = 1$ cell. Quite different sawtooth shapes are observed (figure 16), with slightly different values of $r_{\mathrm{abs}}/r_{\mathrm{inv}}$ [5], according to where the heating is localized with respect to the rotating $m = 1$ island and the sawtooth inversion radius.

6. Conclusions

Localized ECRH is effective in altering the current density profile to the extent of modifying MHD activity. The linear and nonlinear stability of $m = 1$, $n = 1$ perturbations depends on the changes of the local magnetic shear due to the localized ECRH. The dynamics of $m = 2$, $n = 1$ and $m = 1$, $n = 1$ modes obey the local balance between stabilising and de-stabilising forces, including the total stability parameter Δ' from the internal current distribution, the nearby-m mode coupling in toroidal geometry, and the resistive wall braking torque.

The dominant effect around $r_{q=2}$ on energy confinement is a thermal short circuit across the $m = 2, n = 1$ island, while core heating with localized ECRH in the presence of a saturated or reconnecting $m = 1$, $n = 1$ mode may depend on heat conduction/convection inside the asymmetric rotating $m = 1$ island. Further theoretical and experimental investigation of this last point is needed.

Global confinement is largely unaffected by core transport details related to $m = 1$ activity, and is in fair agreement with ITER L-mode scaling laws.

References

[1] Alladio F *et al* 1999 *Plasma Phys. Control. Fusion* **41** A323

[2] Nave M F F, Lazzaro E, Edwards A, Hirsch K, Hugon M, Jacchia A, Salzmann H and Smeulders P 1992 *Nucl. Fusion* **32** 825

[3] Lopez Cardozo N J, Schüller F C, Barth C J, Chu C C, Pijper F J, Lok J and Oomens A A M 1994 *Phys. Rev. Lett.* **73** 256

[4] Porcelli F, Rossi E, Cima G and Wootton A 1999 *Phys. Rev. Lett.* **82** 1458

[5] Pochelon A *et al* 1998 *Proc. 17th IAEA Fusion Energy Conf. (Yokohama, 19–24 October)* at press

[6] Tudisco O *et al* 1999 *Proc. 26th EPS Conf. on Contr. Fusion and Plasma Physics (Maastricht, 14–18 June) (ECA)* ed B Schweer *et al* vol 23J (Geneva: EPS) p 101

[7] Nowak S *et al* 1999 *Proc. 13th Topical Conference on Applications of Radio Frequency Power to Plasmas (Annapolis, 12–14 April)* ed S Bernabei and F Paoletti (Melville: AIP 485) p 269

[8] Krivenski V 1999 *Proc. 26th EPS Conf. on Contr. Fusion and Plasma Physics (Maastricht, 14–18 June) (ECA)* ed B Schweer *et al*, vol 23J (Geneva: EPS) p 385

[9] Cirant S *et al* 1998 *ICPP and 25th EPS Conf. on Contr. Fusion and Plasma Physics (Praha, 29 June–3 July) (ECA)* ed J Stockel *et al*, vol 22C (Geneva: EPS) p 1174

[10] Cirant S *et al* 1998 *Proc. 17th IAEA Fusion Energy Conf. (Yokohama, 19–24 October)* paper IAEA-F1-CN-69/CDP/07, at press

[11] Cirant S *et al* 1999 *Proc. 13th Topical Conf. on Applications of Radio Frequency Power to Plasmas (Annapolis, 12–14 April)* ed S Bernabei and F Paoletti (Melville: AIP 485) p 221

[12] Cirant S *et al* 1998 *Proc. 2nd Europhysics Topical Conf. on Radio Frequency Heating and Current Drive of*

Fusion Devices (Brussels, 20–23 January, 1998) (ECA) ed J Jacquinot, G Van Oost and R R Weynants, vol 22A (Geneva: EPS) p 205

[13] Bruschi A *et al* 1999 *Proc. 26th EPS Conf. on Contr. Fusion and Plasma Physics (Maastricht, 14–18 June) (ECA)* ed B Schweer *et al* vol 23J (Geneva: EPS) p 1177

[14] Ramponi G *et al* 1999 *Proc. 13th Topical Conf. on Applications of Radio Frequency Power to Plasmas (Annapolis, 12–14 April)* ed S Bernabei and F Paoletti (Melvilla: EIP 485) p 265

[15] Lazzaro E *et al* 1999 *Proc. 26th EPS Conf. on Contr. Fusion and Plasma Physics (Maastricht, 14–18 June) (ECA)* ed B Schweer *et al* vol 23J (Geneva: EPS) p 381

[16] Zakharov L E, Levinton F M, Batha S H, Budny R V, Zarnstoff M C, Migliuolo S and Rogers B 1994 *Proc. 15th IAEA Int. Conf. on Plasma Physics and Controlled Nuclear Fusion Research (Seville, 26 September–1 October)* vol 3 (Vienna: IAEA) p 407

[17] Bussac M N, Pellat R, Edery D and Soule J L 1975 *Phys. Rev. Lett.* **35** 1638

[18] Smolyakov A I 1993 *Plasma Phys. Control. Fusion* **35** 657

[19] Thyagaraja A and Haas F S 1991 *Phys. Fluids* B **3** 580

[20] Ara G *et al* 1978 *Ann. Phys.* **112** 443

[21] Buratti P *et al* 1998 *ICPP and 25th EPS Conf. on Contr. Fusion and Plasma Physics (Praha, 29 June–3 July, 1998) (ECA)* ed J Stockel *et al*, vol 22C (Vienna: EPS) p 854

[22] Kaye S M *et al* 1997 *Nucl. Fusion* **37** 1303